Electronic Supplementary Material (ESI) for Materials Horizons.

Supplementary Information

Organic cations promote exciton dissociation in Ruddlesden-Popper lead iodide perovskites: A theoretical study

Xiaohua Tan[1], Qingjie Feng[1], Guangjun Nan[1,2*]

[1] Department of Physics, Zhejiang Normal University, Jinhua, Zhejiang 321004, P. R. China

[2] Zhejiang Institute of Photoelectronics & Zhejiang Institute for Advanced Light Source, Zhejiang Normal University, Jinhua, Zhejiang 321004, P. R. China

[*]Corresponding author, Email: gjnan@zjnu.edu.cn

Text S1.1. TDDFT method for photogenerated electron-hole densities

Following the relaxed ground-state geometry with the combination of the DFT approach and the OTRSH functional described below,[1] a plane-wave TDDFT approach based on the density functional perturbation theory is adopted to calculate the photogenerated the e-h distributions.[2] Specifically, the electronic excitation is determined by solving a non-Hermitian eigenvalue equation

$$\begin{pmatrix} \tilde{A} & \tilde{B} \\ \tilde{B} & \tilde{A} \end{pmatrix} \begin{pmatrix} \tilde{\psi}^{+}_{\alpha} \\ \tilde{\psi}^{-}_{\alpha} \end{pmatrix} = \omega_{\alpha} \begin{pmatrix} -\tilde{S} & 0 \\ 0 & \tilde{S} \end{pmatrix} \begin{pmatrix} \tilde{\psi}^{+}_{\alpha} \\ \tilde{\psi}^{-}_{\alpha} \end{pmatrix} \tag{S1}$$

which is analogous to Casida's equation.[3] Here, $\tilde{\psi}^{\pm}_{\alpha}$ are the linear-response orbitals and ω_{α} is αth excitation energy. The matrix operators $\tilde{A}$ and $\tilde{B}$ that act on the linear-response orbitals can be found elsewhere.[4] Note that the linear-response orbitals are expanded by the plane-wave basis in the virtual space which is orthogonal to the occupied orbitals. To avoid the need to obtain all the virtual orbitals, a projector, $\hat{P}=1-\sum_{i} S|\phi_i\rangle\langle\phi_i|$ with ϕ_i representing the occupied KS orbitals, is used to remove the contribution of the occupied space. In order to guarantee the convergence of the excited-state calculations, the considered occupied orbitals from the highest occupied KS orbitals to the energetically lower occupied KS orbitals should be sufficient.

To calculate the ionic force and the charge density of excited states, we introduce a Lagrangian functional

$$\hat{\mathcal{L}}[x,\tilde{\psi},\tilde{Z},\Gamma] = M_{\alpha\alpha}[x,\tilde{\psi}] + \sum_{ij\sigma} \left\langle \tilde{Z}_{i\sigma} \middle| \left(H^{\sigma}\delta_{ij} - \epsilon_{ij\sigma}\tilde{S}\right) \middle| \tilde{\psi}_{j\sigma} \right\rangle - \sum_{i \geq j,\sigma} \Gamma_{ij\sigma}\left(\left\langle \tilde{\psi}_{i\sigma} \middle| \tilde{S} \middle| \tilde{\psi}_{j\sigma} \right\rangle - \delta_{ij}\right) \tag{S2}$$

by enforcing the Brillouin condition and the orthonormal condition for the KS orbitals, where x denotes the ionic coordinate. Here, we have defined the functional

$$M_{\alpha\alpha} \equiv \begin{pmatrix} \tilde{\psi}^{+}_{\alpha} & \tilde{\psi}^{-}_{\alpha} \end{pmatrix} \left[\begin{pmatrix} \tilde{A} & \tilde{B} \\ \tilde{B} & \tilde{A} \end{pmatrix} + \omega_{\beta} \begin{pmatrix} \tilde{S} & 0 \\ 0 & -\tilde{S} \end{pmatrix} \right] \begin{pmatrix} \tilde{\psi}^{+}_{\alpha} \\ \tilde{\psi}^{-}_{\alpha} \end{pmatrix} \tag{S3}$$

The multipliers $\tilde{Z}$ and Γ can be determined by $\delta\hat{\mathcal{L}}/\delta\tilde{\psi}_i = 0$ which is the stationary condition of the

Lagrangian functional. The ionic force of excited states can then be calculated as the partial derivative of the Lagrangian function with respect to the ionic coordinate $F_\alpha = -\partial\hat{L}/\partial x$. The charge density of the αth excited state can be obtained by the derivative of the Lagrangian functional with respect to the external potential as $\tilde{\rho}_\alpha^{ex} = -\delta\hat{L}/\delta\hat{V}_{ext}$.

Text S1.2. Optimally tuned and range-separated hybrid functional

It has been suggested that the valence band can be reasonably predicted by hybrid functionals which is then combined with spin-orbital coupling (SOC) corrections to calculate the band gap in lead halide perovskites.[5] To reasonably predict the energy level alignment of valence band contributed by organic spacer layers and QWs in 2D RPPs,[6] a recently developed OTRSH functional is resorted in this work.[1] Specifically, the Coulomb repulsion operator $1/r$ is divided into a short-range and a long-range part by using the error function

$$\frac{1}{r} = \frac{\alpha + \beta\mathrm{erf}(\mu r)}{r} + \frac{1 - \alpha - \beta\mathrm{erf}(\mu r)}{r} \quad \text{(S4)}$$

where r denotes the distance between electrons, erf(μr) is the Gaussian error function with μ being a range-separation parameter. The α and β are also tunable parameters and satisfy the requirement of $\alpha + \beta = 1/\varepsilon_0$ where ε_0 represents the static dielectric constant of the solid. The Fock-like exchange and semi-local Kohn-Sham (KS) exchange functional are applied to treat the first and second term at the right-hand side, respectively. Then, the OTRSH exchange correlation (XC) potential is given by

$$V_{xc}^{RSH} = \alpha V_{Fx} + \beta V_{Fx}^{LR} + (1 - \alpha)V_{KSx} - \beta V_{KSx}^{LR} + V_{KSc} \quad \text{(S5)}$$

Here, LR represents the long-range terms, Fx labels Fock-like exchange, KSx and KSc labels semi-local KS exchange and correlation, respectively.

The optimal tuning of these parameters in the OTRSH functional is critical for accurately

evaluating the alignment of inorganic and organic sublevels at the valence band before exploring the role of the organic cations on the hole transport along the normal direction of the QW plane in $(BA)_2(MA)_{n-1}Pb_nI_{3n+1}$ RPPs. In this work, we use α = 0.2 which is a universally valid choice of the short-range exact exchange[7,8] and determine β value ($\boldsymbol{\beta} = \boldsymbol{\varepsilon}_0^{-1} - \boldsymbol{\alpha}$) by adopting ε_0 = 4 which is the out-of-plane dielectric constant of $(BA)_2PbI_4$.[9,10] Considering the primitive cell of $(BA)_2(MA)_{n-1}Pb_nI_{3n+1}$ (n = 1, 2 and 3) includes 156, 204 and 252 atoms, respectively, the range-separation parameter μ is tuned by adopting the computationally feasible scheme: (i) the Perdew-Burke-Ernzerhof (PBE) functional with and without the SOC corrections are combined with the DFT approach to evaluate the band gaps (Fig. S1) the difference (ΔE_{SOC}) of which approximately represents the SOC effect for the band gap in $(BA)_2(MA)_{n-1}Pb_nI_{3n+1}$ (n = 1, 2 and 3);[11] (ii) the μ value for $(BA)_2PbI_4$ is varied to achieve the fundamental band gap which is the sum of the ΔE_{SOC} and the experimentally measured fundamental band gap (2.73 eV) in $(BA)_2PbI_4$.[12] In this way, we determine μ = 0.12 Å^{-1} in $(BA)_2PbI_4$. This μ value is also used in n = 2 and 3 structures due to the comparable SOC effect (Fig. S1) and the slight change of the dielectric constant with n values.[13,14]

The nonlocal Fock-exchange terms give rise to expensive computational cost when applying the OTRSH functionals to large systems with plane-wave basis. To alleviate the computational expense of the Fock-exchange terms, we resort to the recently developed stochastic representations of the OTRSH functional.[15] Specially, we introduce a random linear-response orbital

$$\left|\tilde{\eta}_{\sigma}^{\pm}\right\rangle = \sum_{i} \left|\tilde{\psi}_{i\sigma}^{\pm}\right\rangle \left\langle \tilde{\psi}_{i\sigma} \left| \Im^{1/2} \right| \xi \right\rangle \tag{S6}$$

by using random functions $\xi(r) = \pm \frac{1}{\sqrt{\Delta V}}$ with a random sign at each real-space grid-point, and ΔV is the volume per grid point. The range-separated exchange kernel is also determined stochastically

according to the expression

$$\frac{erf(\mu|r-r'|)}{|r-r'|} = [\![\zeta(r)\zeta^*(r')]\!]_\varphi \tag{S7}$$

Then, by defining the stochastic orbitals

$$|\tilde{\chi}_\sigma\rangle = \zeta(r)|\tilde{\eta}_\sigma\rangle \tag{S8}$$

the Fock-exchange components in Eq. (S1) can be calculated stochastically by

$$\sum_j \langle \tilde{\psi}_{i\sigma} | K_{RSH} | \tilde{\psi}_{j\sigma}\tilde{\psi}^{\pm}_{j\sigma}\rangle = -[\![|\tilde{\chi}^{\pm}_{\sigma}\rangle\langle\tilde{\chi}_\sigma|\tilde{\psi}_{i\sigma}\rangle]\!]_{\xi,\varphi} \tag{S9}$$

where K_{RSH} is range-separated Coulomb kernel. With the stochastic approach, the numerically expensive Convolution integrals of Fock-exchange terms become product and linear combination calculations. For large systems, the method is almost as efficient as a local-potential KS-DFT and KS-TDDFT. In our simulations, 48 occupied KS orbitals are incorporated to guarantee the convergence of photo-induced e-h distributions (Fig. S2), and 2000 stochastic orbitals are sufficient for converging the ground-state energies and band gaps with an error of less than 10 meV (Fig. S3).

Table S1. Experimental cell parameters (Å) of the $(BA)_2(MA)_{n-1}Pb_nI_{3n+1}$ (n = 1, 2 and 3) RPPs. The values in parentheses represent the lattice parameters of the *c* axis in the stretched structures where the distances between organic spacer layers and lead iodide network are enlarged by 1.0 Å with respect to the experimental structures.

$(BA)_2(MA)_{n-1}Pb_nI_{3n+1}$	Lattice parameters (Å)		
n = 1	a = 8.6825	b = 8.8764	c = 27.6014 (31.6014)
n = 2	a = 8.9470	b = 8.8589	c = 39.3470 (43.3470)
n = 3	a = 8.9275	b = 8.8777	c = 51.9590 (55.9590)

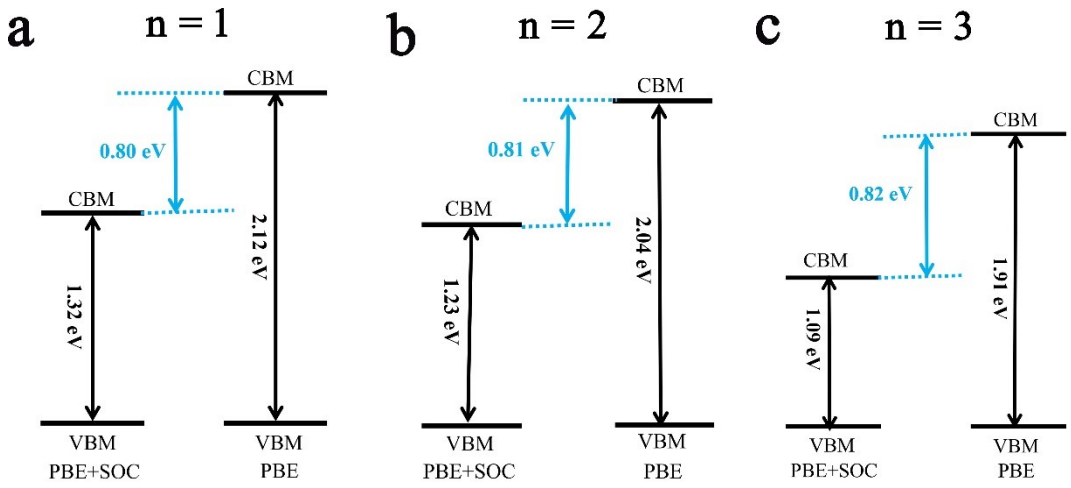

Fig. S1 Calculated band gaps by using the PBE functional with and without the SOC corrections for $(BA)_2(MA)_{n-1}Pb_nI_{3n+1}$. (a) $(BA)_2PbI_4$. (b) $(BA)_2(MA)Pb_2I_7$. (c) $(BA)_2(MA)_2Pb_3I_{10}$. The effect of the SOC corrections is quantified by evaluating the differences of the band gaps at the PBE and PBE+SOC levels.

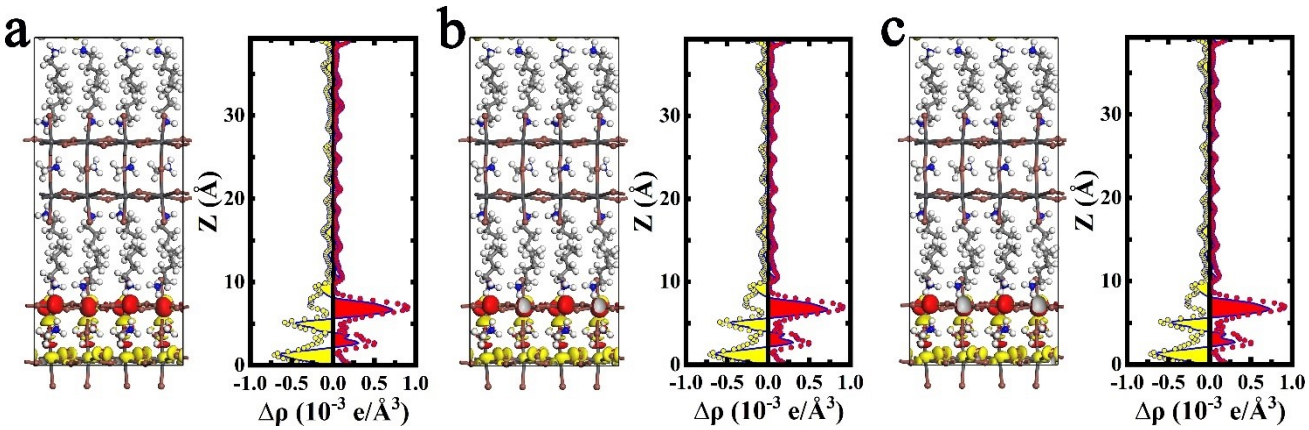

Fig. S2 Photoexcited e-h distributions in the $(BA)_2(MA)Pb_2I_7$ with (15, 30) configuration by including different number (N) of the occupied KS orbitals during the calculations with the TDDFT approach. (a) N = 32. (b) N = 48. (c) N = 64.

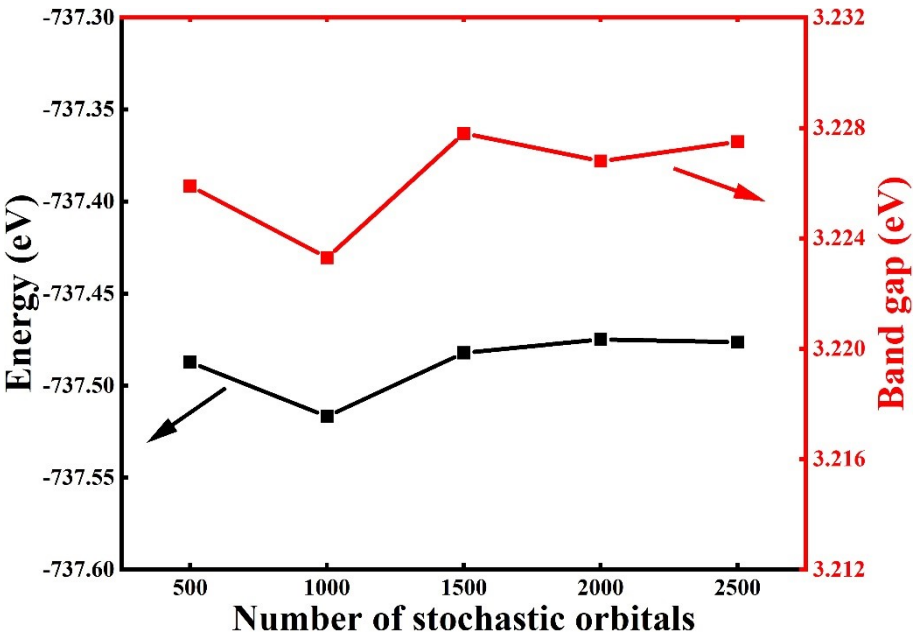

Fig. S3 The change of ground-state energies and band gap with the number of stochastic orbitals needed in the stochastic representations of the OTRSH functional.

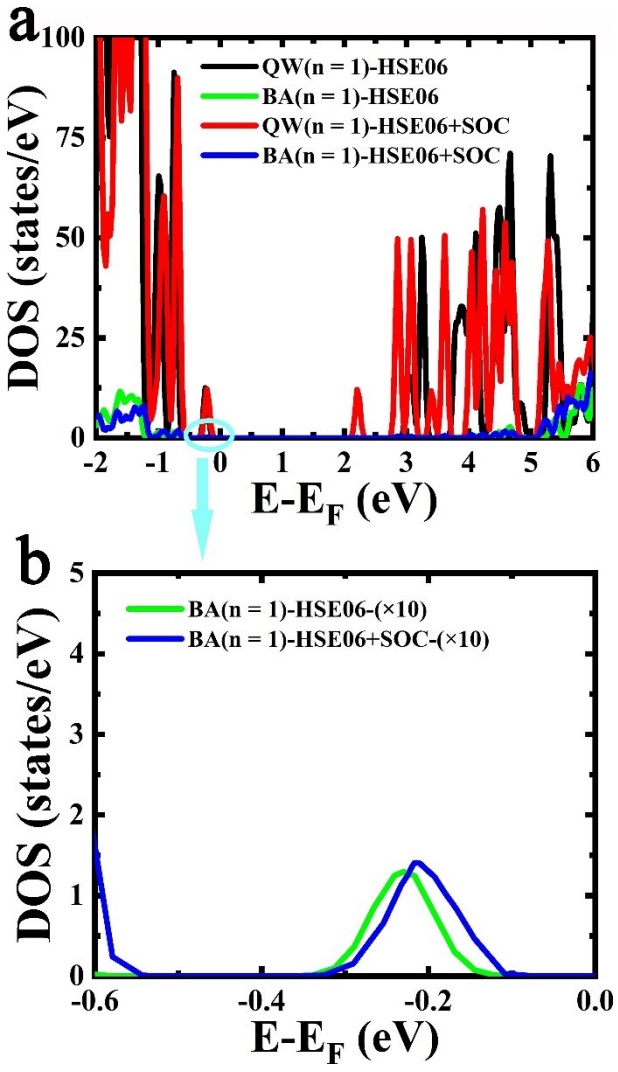

Fig. S4 Calculated DOS of $(BA)_2PbI_4$ by using HSE06 (α = 0.43) functional with and without SOC corrections. (a) DOS of BA cations and inorganic flakes spanning energy window from valence band to conduction band. (b) DOS of the BA ligands at the VBE. In analogy to Fig. 2b, the DOS in (b) is zoomed tenfold.

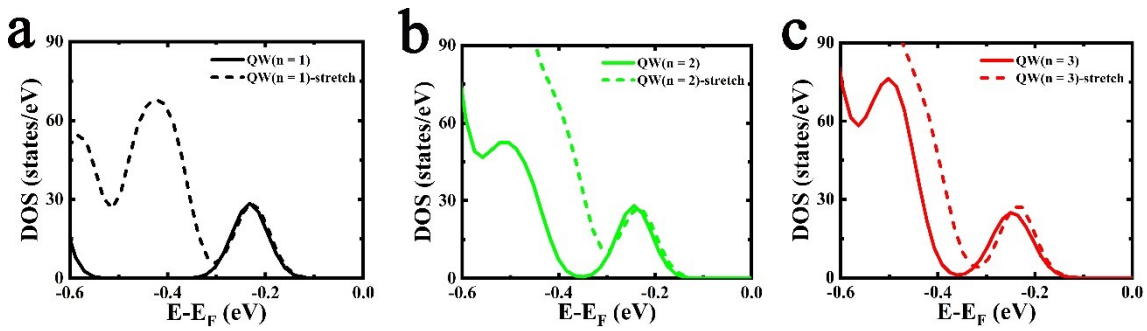

Fig. S5 DOS of VBE contributed by QWs in $(BA)_2(MA)_{n-1}Pb_nI_{3n+1}$ with experimental and stretched lattice parameters in Table S1. (a) $(BA)_2PbI_4$. (b) $(BA)_2(MA)Pb_2I_7$. (c) $(BA)_2(MA)_2Pb_3I_{10}$.

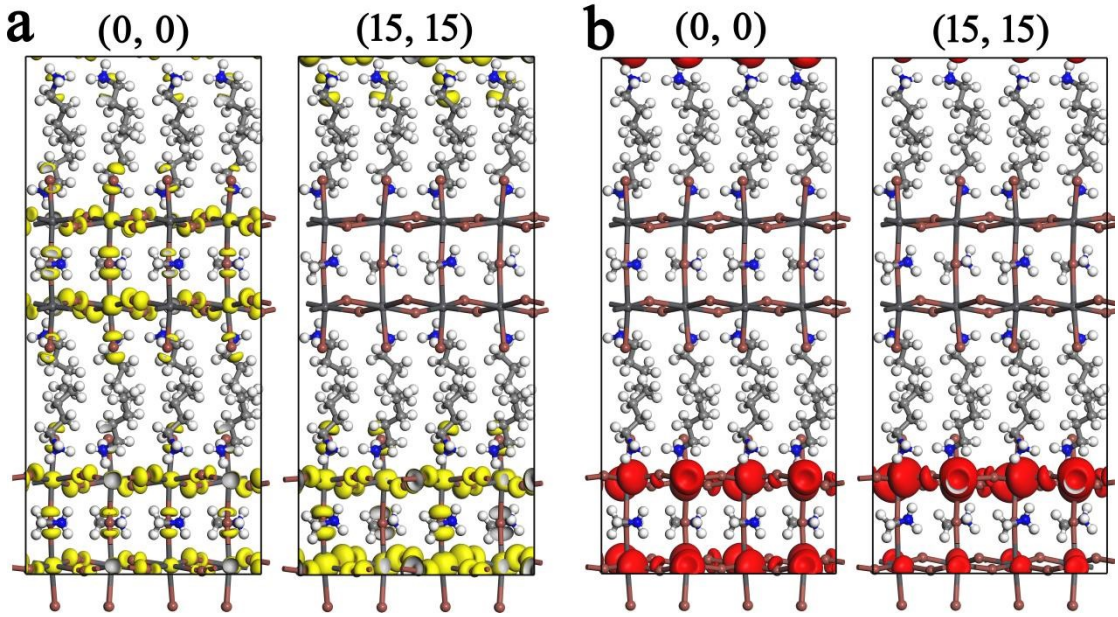

Fig. S6 Frontier orbitals of $(BA)_2(MA)Pb_2I_7$. (a) The highest occupied orbitals in (0, 0) and (15, 15) configurations. (b) The lowest unoccupied orbitals in (0, 0) and (15, 15) configurations. The value of iso-surface is 2.0×10^{-3} e/Å^3 in (a) and (b).

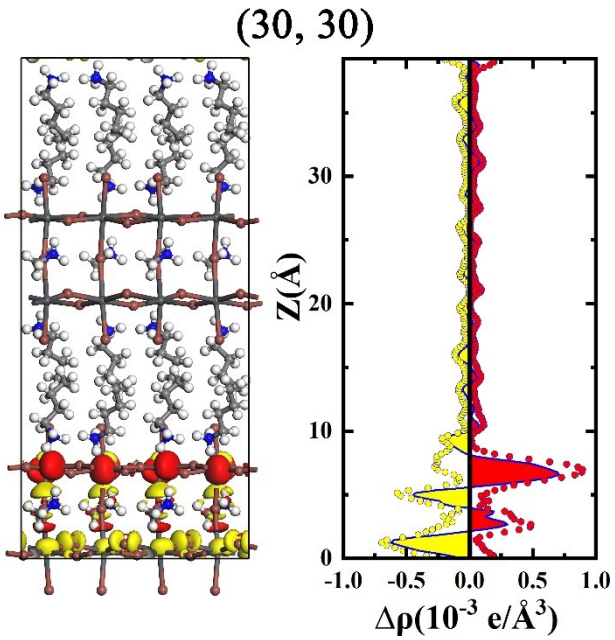

Fig. S7 Photo-induced e-h distributions in the relaxed ground-state geometries of $(BA)_2(MA)Pb_2I_7$ with (30, 30) configuration. The colors and the iso-surface values for exhibiting the electron and hole densities are identical to those in Fig. 3 and 5.

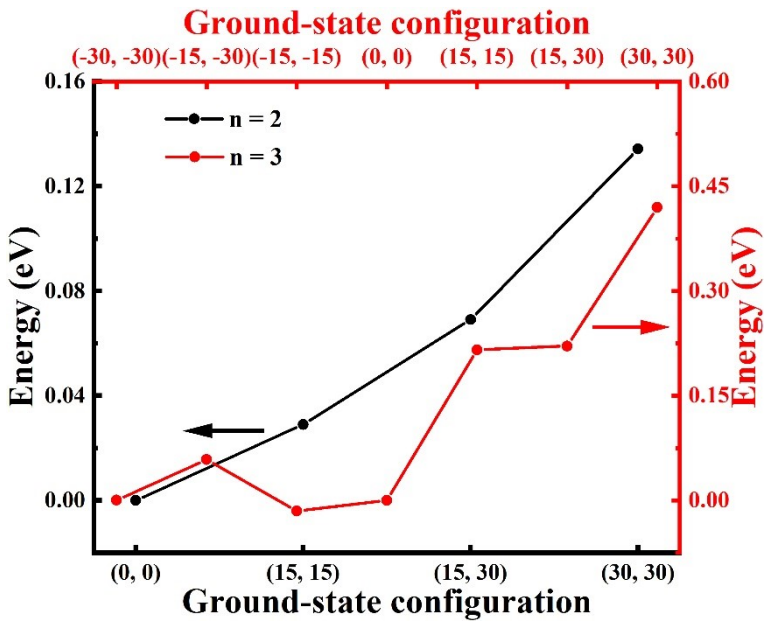

Fig. S8 Relative ground-state energies of $(BA)_2(MA)_{n-1}Pb_nI_{3n+1}$ (n = 2 and 3) with different orientations of the MA cations. The ground-state energies for both n = 2 and 3 structures with (0, 0) configurations are taken as a reference, so the relative ground-state energies defined here are the ground-state energy differences with respect to this reference, divided by the number of primitive cells in the adopted 2×2×1 supercells.

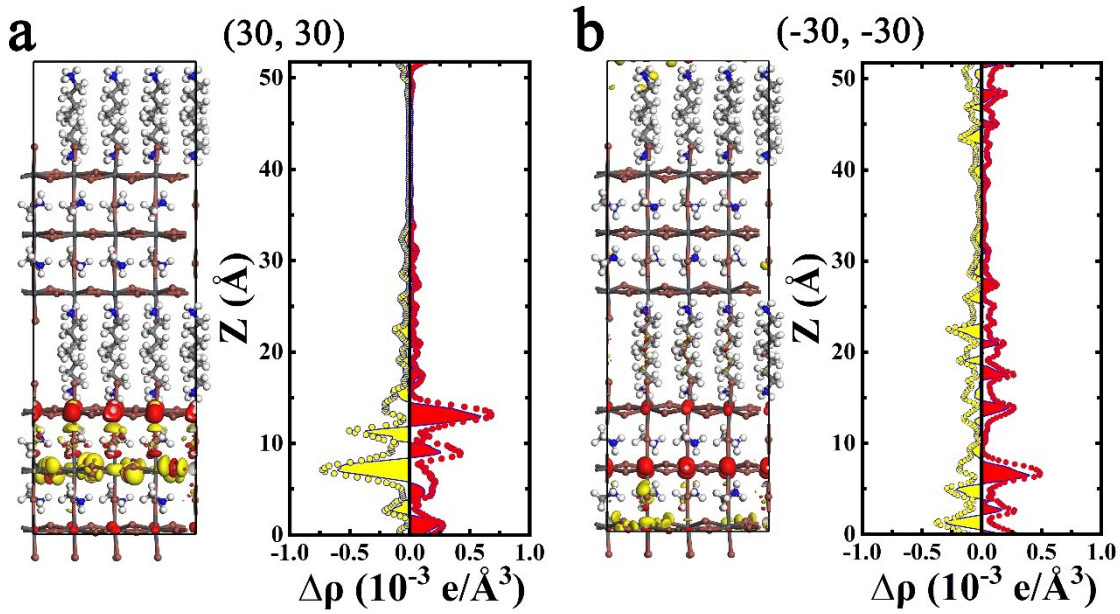

Fig. S9 The light-triggered e-h distributions in $(BA)_2(MA)_2Pb_3I_{10}$. (a) (30, 30) configuration. (b) (-30 -30) configuration. The colors and the iso-surface values for representing the electron and hole carriers in each figure are identical to those in Fig. 3 and 5.

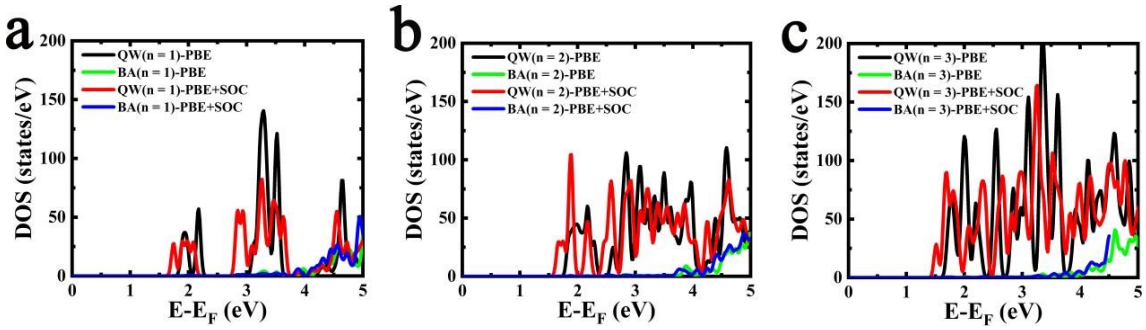

Fig. S10 DOS of conduction band calculated by using the PBE functional with and without SOC corrections for the $(BA)_2(MA)_{n-1}Pb_nI_{3n+1}$ RPPs. (a) $(BA)_2PbI_4$. (b) $(BA)_2(MA)Pb_2I_7$. (c) $(BA)_2(MA)_2Pb_3I_{10}$. The misalignment of the energy levels from BA ligands and QWs is not affected by the SOC effect.

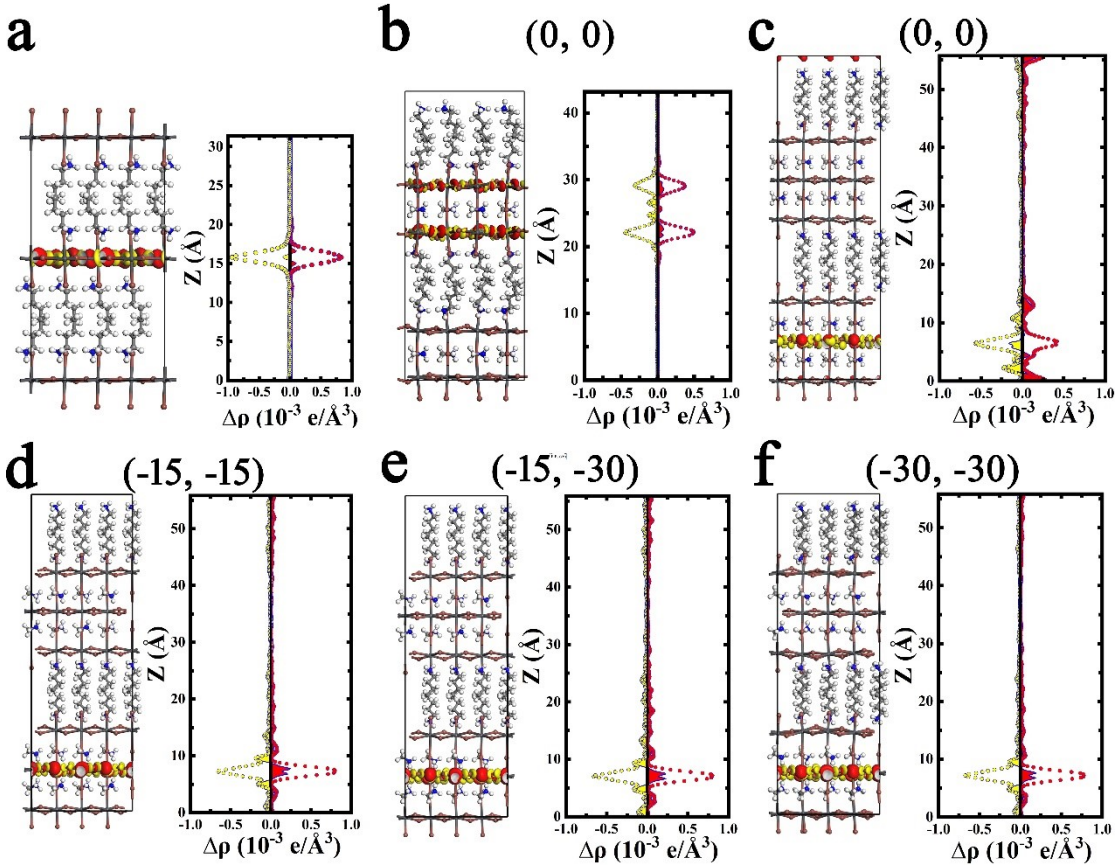

Fig. S11 The photoexcited e-h densities in the stretched structures (Table S1) of $(BA)_2(MA)_{n-1}Pb_nI_{3n+1}$ RPPs. (a) $(BA)_2PbI_4$. (b) $(BA)_2(MA)Pb_2I_7$ in (0, 0) configuration. (c-f) $(BA)_2(MA)_2Pb_3I_{10}$ in (0, 0), (-15, -15), (-15, -30) and (-30, -30) configuration, respectively. In each figure, the colors and the iso-surface values for presenting the electron and hole carriers are identical to those in Fig. 3 and 5.

Reference

1 S. Refaely-Abramson, M. Jain, S. Sharifzadeh, J. B. Neaton and L. Kronik, *Phys. Rev. B*, 2015, **92**, 081204(R).

2 X. Zhang and G. Lu, *J. Chem. Phys.*, 2015, **143**, 064110 .

3 M. E. Casida, in *Recent Advances in Density Functional Methods*, ed. D. P. Chong, World Scientific, Singapore, 1995, pp. 155-192.

4 X. Zhang, Z. Li and G. Lu, *J. Phys.: Condens. Matter.*, 2012, **24**, 205801.

5 M.-H. Du, *J. Phys. Chem. Lett.*, 2015, **6**, 1461-1466.

6 N. Marchal, E. Mosconi, G. García-Espejo, T. M. Almutairi, C. Quarti, D. Beljonne and F. De Angelis, *J. Phys. Chem. Lett.*, 2021, **12**, 2528-2535.

7 M. A. Rohrdanz, K. M. Martins and J. M. Herbert, *J. Chem. Phys.*, 2009, **130**, 054112.

8 D. A. Egger, S. Weissman, S. Refaely-Abramson, S. Sharifzadeh, M. Dauth, R. Baer, S. Kümmel, J. B. Neaton, E. Zojer and L. Kronik, *J. Chem. Theory Comput.*, 2014, **10**, 1934-1952.

9 Y. Gao, M. Zhang, X. Zhang and G. Lu, *J. Phys. Chem. Lett.*, 2019, **10**, 3820-3827.

10 L. Pedesseau, M. Kepenekian, D. Sapori, Y. Huang, A. Rolland, A. Beck, C. Cornet, O. Durand, S. Wang and C. Katan, *Physics, Simulation, and Photonic Engineering of Photovoltaic Devices V*, SPIE, 2016, 9743, 86-94.

11 M. R. Filip and F. Giustino, *Phys. Rev. B*, 2014, **90**, 245145.

12 E. Amerling, S. Baniya, E. Lafalce, C. Zhang, Z. V. Vardeny and L. Whittaker-Brooks, *J. Phys. Chem. Lett.*, 2017, **8**, 4557-4564.

13 B. Traore, L. Pedesseau, L. Assam, X. Che, J.-C. Blancon, H. Tsai, W. Nie, C. C. Stoumpos, M. G. Kanatzidis, S. Tretiak, A. D. Mohite, J. Even, M. Kepenekian anad C. Katan, *ACS Nano*, 2018, **12**,

3321-3332.

14 J.-C. Blancon, A. V. Stier, H. Tsai, W. Nie, C. C. Stoumpos, B. Traoré, L. Pedesseau, M. Kepenekian, F. Katsutani, G. T. Noe, J. Kono, S. Tretiak, S. A. Crooker, C. Kantan, M. G. Kanatzidis, J. J. Crochet, J. Even and A. D. Mohite, *Nat. Commun.*, 2018, **9**, 2254.

15 X. Zhang, G. Lu, R. Baer, E. Rabani and D. Neuhauser, *J. Chem. Theory Comput.*, 2020, **16**, 1064-1072.